

# SELECTIVE LASER MELTING OF POROUS STRUCTURES

H. A. Stoffregen<sup>1</sup>, J. Fischer<sup>1,2</sup>, C. Siedelhofer<sup>1</sup>, E. Abele<sup>1,2</sup>

1) Institute of Production Management, Technology and Machine Tools (PTW), Technische Universität Darmstadt, Germany

2) Center of Smart Interfaces (CSI), Technische Universität Darmstadt, Germany

REVIEWED, August 17 2011

## **Abstract**

Within the Center of Smart Interfaces “Understanding and Designing Fluid Boundaries”, a German Excellence Initiative, the Institute of Production Management, Technology and Machine Tools examines the manufacturing of porous structures by using selective laser melting (SLM). In this paper two different strategies are presented in order to obtain porosity: One strategy is to manufacture geometrically defined lattice structures. SLM allows here complex geometries that cannot be manufactured by conventional technologies to be built. The second approach is to manufacture geometrically undefined porosity by a specific modification of exposure parameters. The SLM generated porous structures are investigated with respect to the heat and mass transfer. The research focus is to increase the efficiency of spraycooling effects and the manipulation of the Leidenfrost point.

## **Introduction**

The Cluster of Excellence “Smart Interfaces – Understanding and Designing Fluid Boundaries” has been founded in November 2007 at the Technische Universität Darmstadt as part of the Excellence Initiative of the federal government of Germany. The Center of Smart Interfaces focuses on phase interfaces at which fluidic phases (gas and/or liquid) interact with a solid surface. Such fluid-solid interfaces and the associated interfacial phenomena are ubiquitous in our daily lives and represent key technologies in many established and emerging fields. The major research goals of this Cluster encompass the understanding, design, development and application of Smart Interfaces, in particular in the physical and engineering sciences.

The Institute of Production Management, Technology and Machine Tools (PTW) as a member of the Center of Smart Interfaces focuses on the manufacturing of functional surfaces. Within this scope the possibilities of selective laser melting relating to the fabrication of porous surface structures are investigated. The purpose of porous surface structures is to influence spray cooling effects and the Leidenfrost Point.

Porosity is a widely known phenomenon especially in the field of additive manufacturing [1, 2]. In most cases the appearance of porosity is a side effect that has to be minimized because it affects material properties such as strength, hardness and surface quality negatively [3]. The research on additive manufacturing and specifically on selective laser melting therefore emphasizes on the manufacturing of very dense parts and the avoidance of any porosity [4, 5, 6]. Nevertheless, porous structures have major technical applications. In the field of lightweight construction the presence of porosity can significantly reduce the weight [7]. Thus, by employing

porous structures to load-bearing parts of the automotive or aerospace industry both economic and ecologic advantages can be achieved. Another technical application is the use as medical implants. Porosity is an important characteristic in order to improve the engraftment of implants to existing bone and tissue structures. Due to the fact that biological materials have a specific porosity it is important that the implant's material is showing similar properties. A third technical application represents filters and deaeration components [8, 9]. The function of these components is the permeability for a certain type of gaseous or liquid particles. Therefore, a specific porosity is required.

For the mentioned technical applications it is worthwhile to analyze the manufacturing possibilities of defined porous structures. In this paper the use of selective laser melting will be examined in order to build up samples with a defined porosity. Selective laser melting as a well-established additive manufacturing technology seems to offer several advantages in this context. First, through variation of process parameters such as laser power, scan speed, and hatch distance a partial melting of the metal powder and hence geometrically undefined porosity can be accomplished. The influence of the parameter variation on porosity as one possible strategy will be addressed in this paper. Second, selective laser melting allows complex lattice structures which cannot be manufactured by conventional technologies to be built. This may be a second possibility to manufacture defined porosity and will be analyzed in this paper as well. Porous samples using lattice structures will be called geometrically defined porosity. A particular interest lies in the characterization of the developed porous structures.

## **Methodology**

In this study selective laser melting (SLM) is used to fabricate samples with a defined porosity. Therefore several parameter variations and two geometrically defined lattice structures are tested for being capable to create such a porous structure. Geometrically undefined porosity is to be produced by variation of exposure parameters and geometrically defined structure by the creation of a complex lattice structure.

The examined parameters for geometrically undefined porosity are shown in Figure 1. All of them affect the volume energy density by contributing to the amount of energy that is transported into the material. [10] use a term called linear energy density, which includes only scan speed and laser power. In this study the equation is extended to include the energy per volume. Hence, the volume energy density is defined by:

$$E = \frac{P_L}{v_s \cdot h_s \cdot s}.$$

Where  $P_L$  is the laser power,  $v_s$  the scan speed,  $h_s$  the hatching distance and  $s$  the layer thickness. A lower laser power and higher scan speed, hatching distance and layer thickness decrease the amount of energy, which induces heat into the powder in order to melt it. Since the existence of a fully melted pool is meant to be an important factor to fabricate fully dense structures, a lower energy density should lead to porosity [11]. In this study the influence of the volume energy density on the porosity is studied by the variation of the four different exposure parameters: laser power ( $P_L$ ), scan speed ( $v_s$ ), hatching distance ( $h_s$ ), and layer thickness ( $s$ ). It is

suggested that a decrease in volume energy density leads to porous structures. Until today this relationship is mentioned by many authors. Nevertheless, a definite and characteristic shape of this influence has not been described accurately [12]. In this paper an inversely proportional relation between volume energy density and the obtained porosity  $\varepsilon$  is proposed:

$$\varepsilon = k \cdot \frac{1}{E} = k \cdot \left( \frac{v_s \cdot h_s \cdot s}{P_L} \right)$$

For analysis in this paper one process parameter is being varied while the others remain constant at their standard values. The standard values represent the default set of parameters according to the manufacturer's information. In this way the influence of one single parameter can be identified. The intention is to examine whether there are different influences of these parameters on the porosity and especially to characterize the porosity formed by those parameters. The laser power is varied from the standard 195 to 70 W in ten steps, the scan speed from 1000 to 4500 mm/s in five steps, the hatching distance from 100 to 600  $\mu\text{m}$  in five steps and the layer thickness from 20 to 80  $\mu\text{m}$  in three steps.

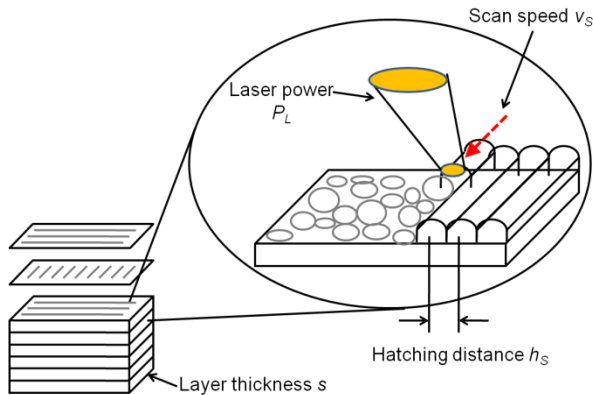


**Figure 1: Schematic process and varied parameters**

The second way to create porosity is the fabrication of a geometrically defined lattice structure. Therefore, two different structures, a honeycomb shaped and a crossing walls structure (Figure 2), are examined – each at different configurations (Figure 8). [13] examine an octahedral structure to fabricate porous bone in-growth structures and find this a promising way, which requires further investigations. [14] use a similar crossing walls structure but apply larger pore sizes, which are tried to be minimized in this study. These attempts show that there is the possibility to fabricate porous parts with lattice structures. This will be examined further in this study. The investigation focuses on the possibilities to fabricate small structures and walls to create porous parts. Furthermore, it will be analyzed whether the desired porosity and pore size given by the theoretical geometry of the structures can be manufactured reliably. The walls are produced with thicknesses of 100 and 200  $\mu\text{m}$  and the characteristic values for the pore channels (pore diameter) are examined from 200 to 400  $\mu\text{m}$  for the honeycomb structures. For the crossing walls structures the distance between the walls is the determining parameter which defines the pore size. It is varied in the range of 100 to 300  $\mu\text{m}$ . The largest pores are in both structures in direction of the z axis. In addition, the crossing walls structure has smaller pores in direction of the x and y axis, which are generated by variation of height and overlap (Figure 2). Those two

parameters are kept constant for this study at values of 200 and respectively 40  $\mu\text{m}$ . Hence, an additional pore volume compared to the honeycomb structure is expected. These pores are applied to evaluate the possibility regarding the manufacturing of multidirectional pores.

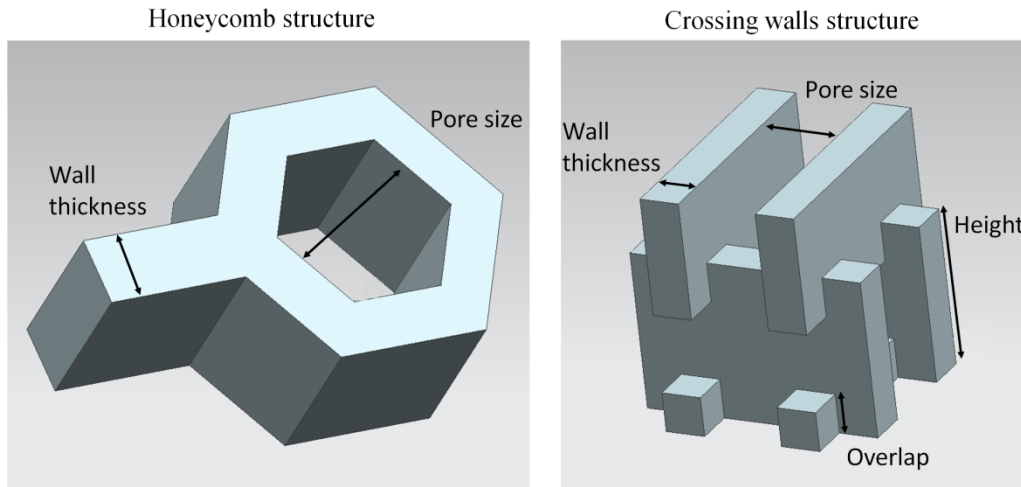


**Figure 2: Geometrical shape and parameters of used lattice structures**

In order to characterize the pore structure, it will be distinguished between open and total porosity. There are two types of open pores, blind and through pores. Both types have a connection to the surface and can be filled by fluids. Closed pores on the other hand are surrounded by fully dense material and have no connection to the surface. Together open and closed pores form the total porosity (Figure 3). Depending on the purpose only closed or open pores are desired to exist in the material. That is the reason why it is important to distinguish between the different types of pores.

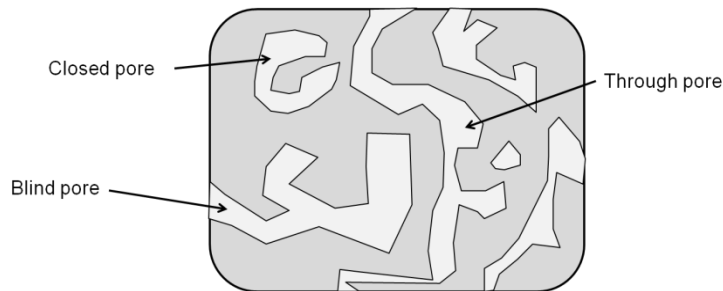


**Figure 3: Three different types of pores**

For the measurement of the total porosity  $\varepsilon$ , both the density of the sample  $\rho_{Sample}$  and the material standard density  $\rho_{Standard}$  are required.  $\rho_{Sample}$  is obtained by the specimen's weight and its volume calculated by the geometrical data. The total porosity  $\varepsilon$  is calculated as follows:

$$\varepsilon = 100 \% \cdot \left( 1 - \frac{\rho_{Sample}}{\rho_{Standard}} \right).$$

For the analysis of the open porosity  $\varepsilon_o$  the solids volume  $V_s$  has to be determined. This is carried out by the Archimedes method [15], where all open pores have to be filled with a liquid<sup>1</sup>. The specimens are weighed surrounded by the liquid ( $m_l$ ) and afterwards in air ( $m_a$ ). With those values and the known density of the liquid ( $\rho_l$ ) the solids volume is calculated as follows:

$$V_s = \frac{m_a - m_l}{\rho_l}.$$

With the solids volume and the theoretical volume  $V_t$  calculated by the geometry of the sample part the open porosity can be determined:

$$\varepsilon_o = 100 \% \cdot \left(1 - \frac{V_s}{V_t}\right).$$

These calculations and the pore size analysis with a mercury intrusion porosimeter allow a comprehensive characterization of the sample parts' porosity.

### **Experimental Setup**

For the production of the sample parts a laser melting station M270 of the company EOS GmbH (Germany) is used. Regarding future technical applications a commercially available stainless steel powder (US: 17-4 PH; EU: 1.4542) is chosen. A set of cylindrical test specimens of 10 mm height and 14 mm diameter are produced. This shape and height of 10 mm respective diameter of 14 mm is chosen to meet the requirements of the measurement instruments. The mercury porosimeter as an example requires specimens that are almost as big as the sample chamber itself to assure reliable results.

For geometrically undefined porosity the exposure parameters are kept constant at the standard value except for the one parameter that is varied. A special contour exposure or post processing is not applied to the test parts in order to minimize side effects that may influence the results. The process uses a continuous wave Yb-fiber laser with a wavelength of 1064 nm and a spot size of 200  $\mu\text{m}$ . Furthermore, Argon acts as a shielding gas in the process chamber.

An ultrasonic bath is used to clean the specimens and remove powder rests from the open pores. For the porosity analysis the samples are weighed with a high precision balance and their volume is calculated by the geometric data.

To measure the open porosity the Archimedes method including weighing both under water and on the air [15] is applied. To fill the pores deionized water is used, in which the samples are boiled for one hour. In order to characterize the pore size distribution a mercury porosimeter is used (Autopore IV 9500 by Micromeritics, Germany). For this method non wetting mercury is used to fill the pores of the test samples. The intrusion volume at different pressure levels is measured. Afterwards the corresponding pore diameter is calculated by the Washburn-Equation. The output leads to the pore distribution over a specified range of pore diameters. With the used equipment pore sizes starting from 1 nm up to 150  $\mu\text{m}$  can be detected

---

<sup>1</sup> The use of any wetting liquid is possible, in this study deionized water is used.

with this measurement method [16, 17]. In addition, the conformance of the theoretical values for inner structures and pores of the honeycomb and lattice structures is analyzed. Therefore a light-optical microscope is used.

## Results

The results of the porosity analysis for geometrically undefined porosity are shown in Figure 4. A negative correlation between laser power and porosity can be seen. The highest porosity is reached at the lowest laser power of 70 W (17.65 %). Below this power it is not possible to fabricate solid specimens. The correlation seems to have an exponential relation. The rise of the other three parameters has a positive effect on the porosity. By increasing the scan speed a porosity up to 27.03 % is possible (at 4500mm/s), whereas the hatching distance allows values up to 36.02 % (at 600  $\mu\text{m}$ ) and the layer thickness up to 11.44 % (at 80  $\mu\text{m}$ ). The relation between scan speed and porosity respective hatching distance and porosity has a linear shape, whereas the one between layer thickness and porosity has an exponential shape. The regression curves for total porosity are included in the diagrams with their coefficient of determination ( $R^2$ ). Values of  $R^2$  for all functions are above 0.9 and hence the regression line approximates the real data points very well and the goodness of fit is on a reliable level.

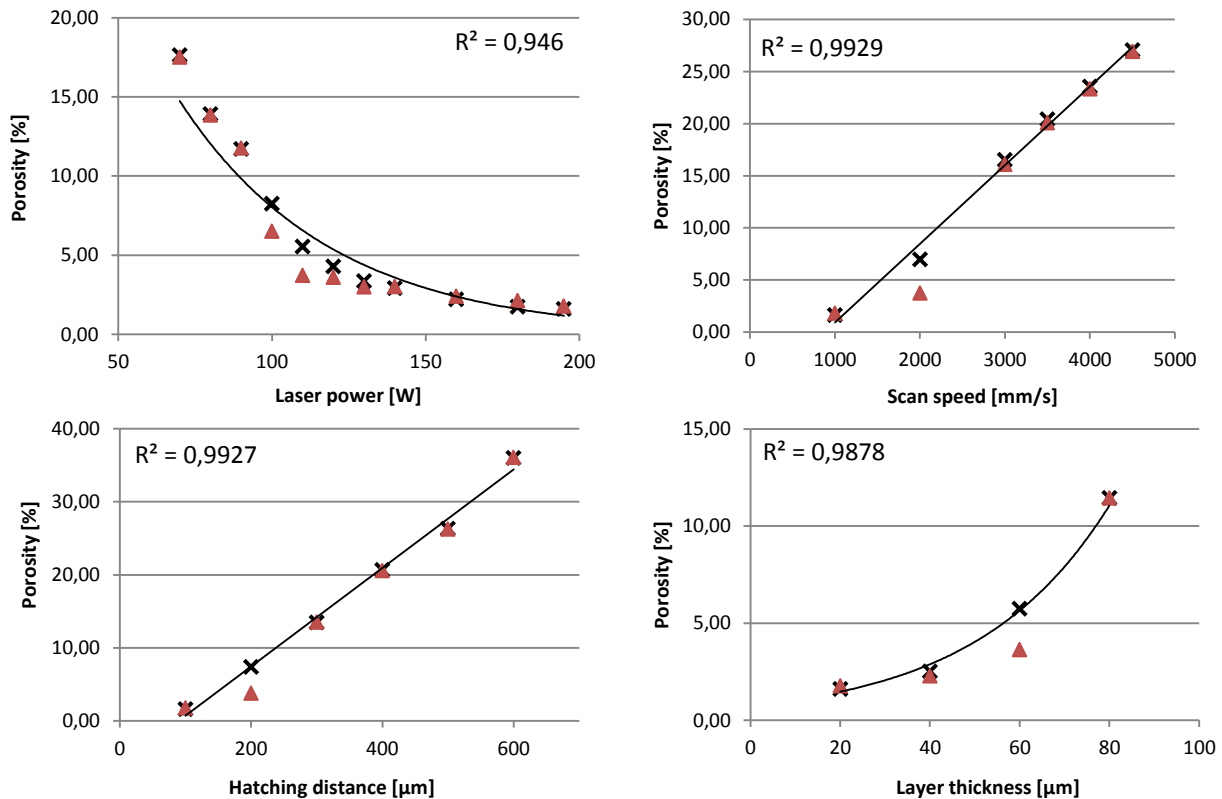


**Figure 4: Influence of the parameter settings on the porosity (black crosses for total porosity, red triangles for open porosity)**

Figure 5 shows the pore size distributions of the investigated parameters. The results are shown in separate diagrams for each parameter to see the changes by variation of the single parameter. The differential intrusion volume is plotted over the pore size diameter. In this way the contribution of each single pore diameter to the open porosity can be determined.

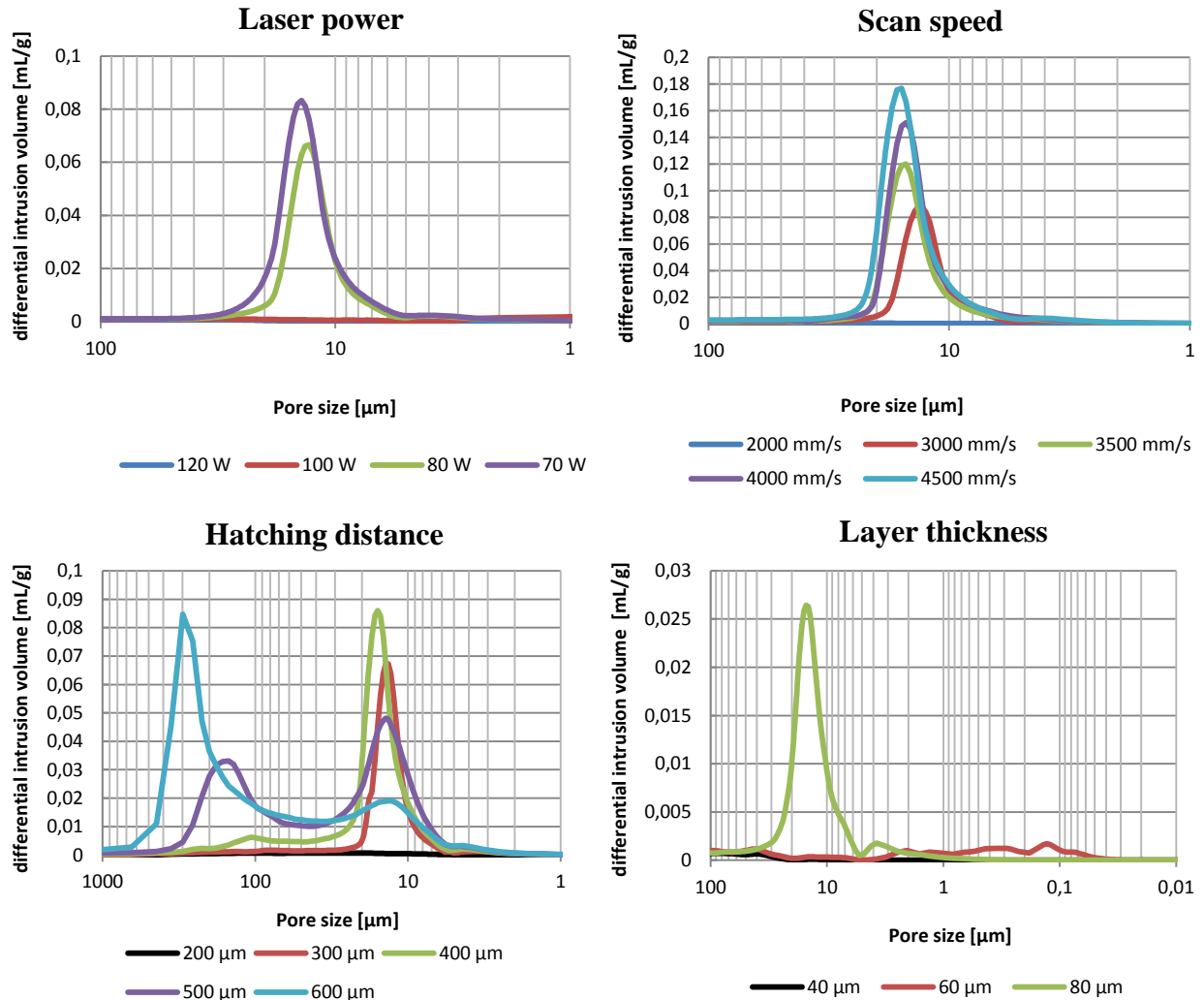
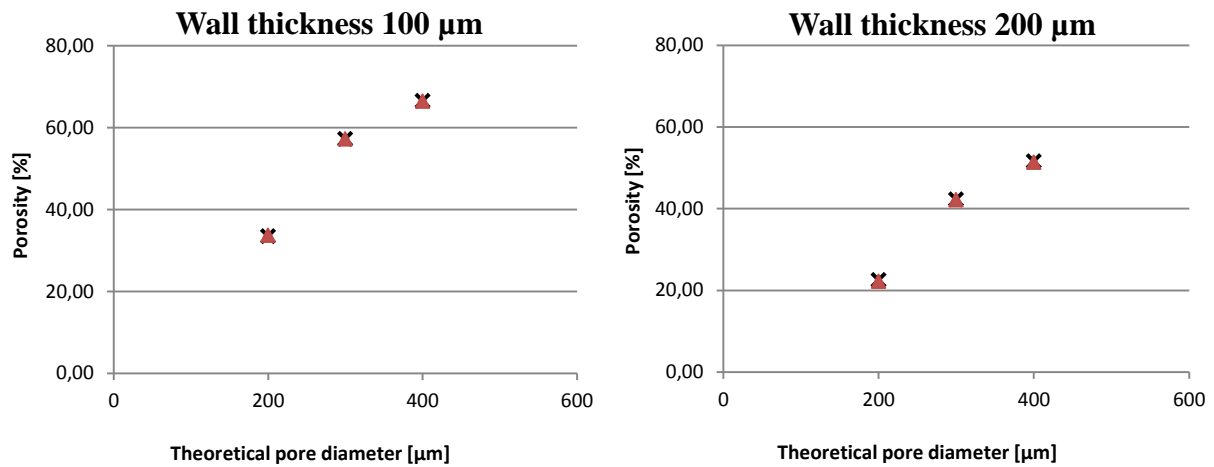
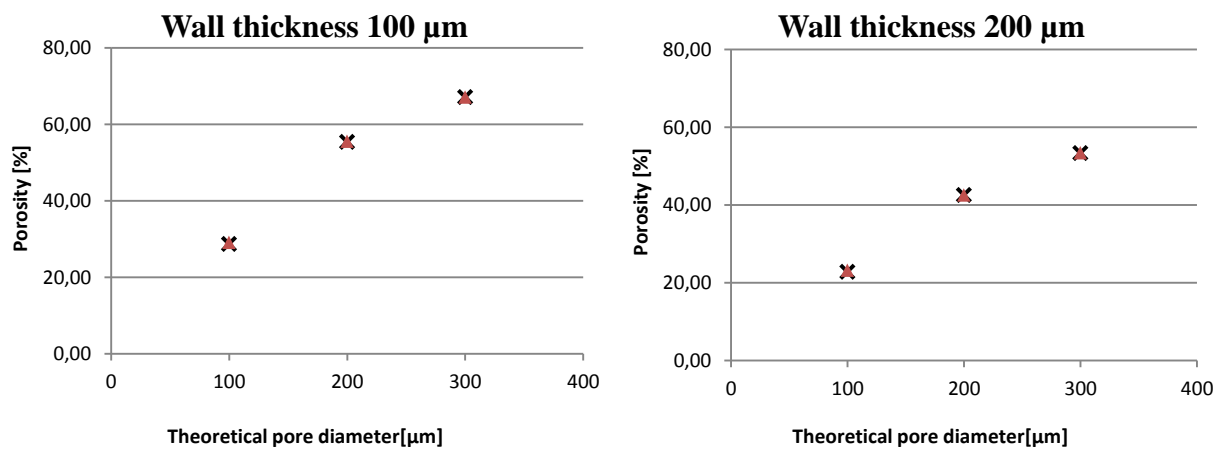


Figure 5: Pore size distribution for each parameter variation at a logarithmic scale

The porosity of the samples with lattice structures (geometrically defined porosity) is shown in Figure 6 and Figure 7. The values for the crossing walls structure and honeycomb structures are outlined over the theoretical pore size. The theoretical pore size is determined by the geometry of the lattice structures. The values for each configuration are listed in Figure 8. It can be seen that a higher wall thickness results in lower porosity and that the porosity correlates with the theoretical pore sizes as well.



**Figure 6: Influence of the configuration values of the honeycomb structure on porosity (on the left wall thickness 100 μm (H1, H2, H3), on the right 200 μm (H4, H5, H6))**



**Figure 7: Influence of the configuration values of the crossing walls structure on porosity (on the left wall thickness 100 μm (CW1, CW2, CW3), on the right 200 μm (CW4, CW5, CW6))**

Figure 8 shows a comparison between the theoretical porosity ( $\epsilon_{theoretical}$ ) and the by selective laser melting achieved porosity ( $\epsilon_{achieved}$ ) for the samples with inner structures. In Figure 9 the resulting pore size distribution for the different configurations is pointed out.

Structure	w all thickness [ $\mu\text{m}$ ]	theoretical pore size [ $\mu\text{m}$ ]	$\epsilon_{\text{theoretical}}$ [%]	$\epsilon_{\text{achieved}}$ [%]	
Honeycomb	H1	100	200	44,44	33,46
	H2	100	300	56,25	57,23
	H3	100	400	64,00	66,56
	H4	200	200	25,00	22,51
	H5	200	300	36,00	42,23
	H6	200	400	44,44	51,6
-----					
Crossing w alls	CW1	100	100	43,75	28,77
	CW2	100	200	61,11	55,43
	CW3	100	300	70,31	67,14
	CW4	200	100	27,78	22,83
	CW5	200	200	43,75	42,57
	CW6	200	300	54	53,39

Figure 8: Comparison between theoretical and achieved porosity values for the samples with geometrically defined lattice structures

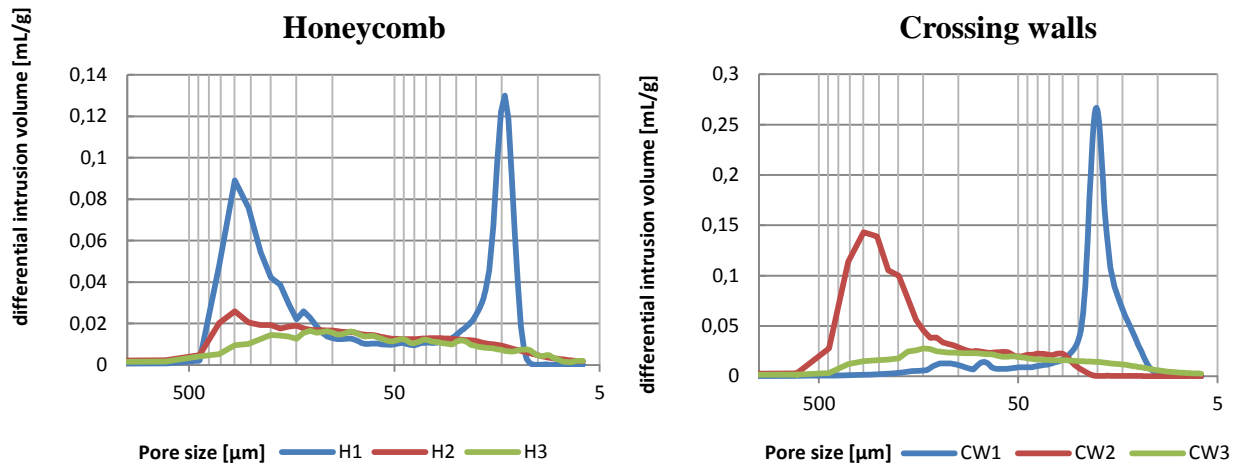
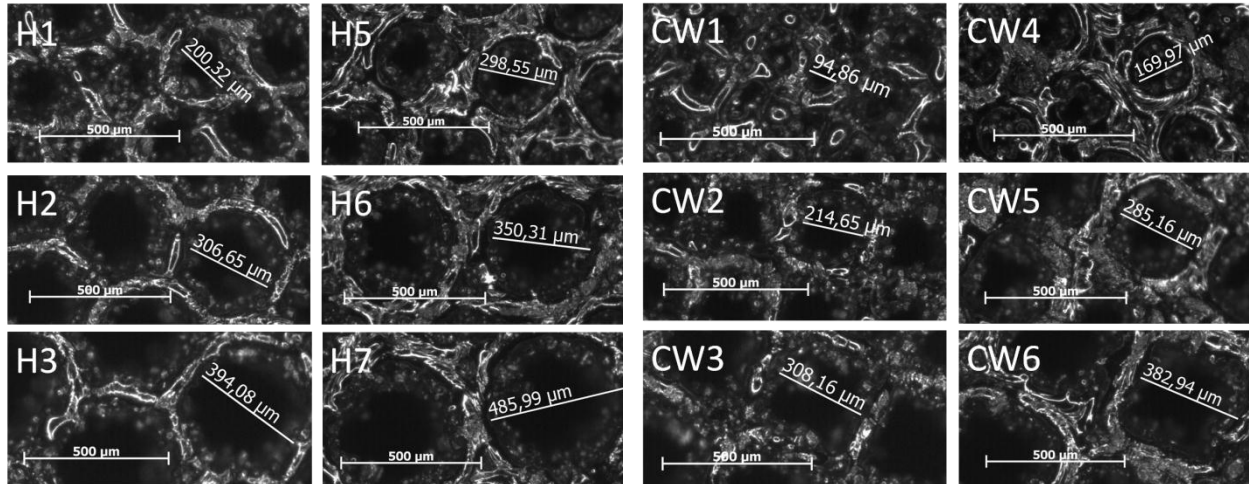


Figure 9: Pore size distribution of the samples with lattice structures (wall thickness 100 $\mu\text{m}$ ; honeycombs on the left, crossing walls on the right) at a logarithmic scale

The results of the microscopic analysis of the inner structures are shown in Figure 10. It can be observed, that the walls with 200  $\mu\text{m}$  thickness are produced by two scan tracks, while the ones with only 100  $\mu\text{m}$  need only one scan track.



**Figure 10: Microscopic view on the produced structures (on the left honeycomb structures; on the right crossing walls structures)**

### Discussion

The presented results allow comprehensive insights into the manufacturing of defined porosity with selective laser melting. With respect to geometrically undefined porosity, a significant correlation between each varied parameter and the resulting porosity can be found as it was expected due to a variance in the applied volume energy density to the powder.

By increasing the laser power porosity values up to 17.65 % are reached. Starting at 195 W only a small increase in porosity can be detected until a laser power of 120 W. Analysis shows that open pores are dominating in this parameter window. In sequel the porosity begins to increase more rapidly and closed pores are detected. This leads to the conclusion that until a laser power of 120 W the test parts just show a higher surface roughness which causes open pores but no closed pores. Below a laser power of 120 W the volume energy density does not suffice to create a fully melted pool. Hence, the effect of solid phase sintering overcomes the liquid phase sintering and by forming small necks between the grains, closed inner pores start to appear [10]. With a further decrease in laser power the inner pores obtain connections to the surface. They become open pores and can be detected by the mercury intrusion porosimetry. Figure 5 shows a first peak at 80 W laser power, when the porosity consists only of open pores. With a laser power below 80 W the pore size is increasing and the porosity rises. The effect of laser power on the porosity seems to have an exponential shape. Considering the almost constant porosity until a laser power of 120 W a linear regression in the range of 120 W to 70 W is suitable as well. Thus, in this range the theory of an inversely proportional influence of the volume energy density on porosity can be supported. Nevertheless, analyzing to complete range of laser power this theory does not hold. A reason for the rather exponential than linear structure might be the lower absorption rate of the material at lower energies and temperatures [18]. Summing up, the porosity can be influenced by the laser power in a modest range from 1.75 to 17.65 %, while the porosity consists mainly out of open pores. The pore size can be influenced slightly in a range from 10 to 30  $\mu\text{m}$ .

The regression line of scan speed on porosity has a linear shape. This supports the proposed inversely proportional relation between laser energy density and porosity (Figure 4). A porosity up to 27.03 % can be accomplished through a variation of the scan speed before the test-specimens lose cohesion. The porosity, which appears at the first increase of scan speed consists almost to 50 % of closed pores (Figure 4). The detected open porosity is a result of the higher surface roughness. The closed pores in the test parts are caused by a lower volume energy density. A critical scan speed at which pores start to grow and which results in the existence of lateral pores parallel to the scan track is also found by [19]. With further increase of scan speed, pores start growing in the material and getting connection to the surface. Hence, the closed porosity decreases and at scan speeds above 3000 mm/s nearly all of the porosity consists of open pores. This is the result of a rapid pore growing. The porosity continues growing linear with the scan speed. The pore distribution shows quite well formed peaks with a Gaussian distribution, which is important for a defined influence on pore diameters. The mean value rises with an increase of the scan speed at a constant rate from 12 to 18  $\mu\text{m}$ . This allows a good influence both on the porosity and the mean pore size. The significant shift of the mean pore diameter with increasing scan speed can be explained by a shorter time interval, during that liquid phase sintering occurs. The material is a shorter time in the liquid phase and cannot close the pores between the grains. As it becomes solid more rapidly only the small gaps can be filled, bigger ones cannot be covered by the melting pool. In addition a shorter liquid phase keeps gas bubbles in the molten pool from rising up to the surface. They are trapped in the material and form porosity. A shorter time of liquid phase thereby causes a shorter time span for the bubbles to escape out of the material. Hence, the scan speed is considered to be an effective way to control the level of porosity from 6.96 to 27.03 % and pore sizes in the small range from 12 to 18  $\mu\text{m}$ .

The hatching distance as the third analyzed parameter allows porosity values up to 36.02 %. Even a further increase of porosity might be possible but has not been investigated within this study. The parameter has a linear influence on the porosity (Figure 5), which matches the assumption that the volume energy density influences the porosity inversely proportionally. As seen at the already discussed parameters, closed porosity mainly exists at the beginning of an increase of hatching distance. Closed porosity and also the detected open porosity in the size of 5 to 20  $\mu\text{m}$  at a hatching distance of 300  $\mu\text{m}$  can be explained by the same mechanisms as before. An increasing hatching distance causes a decreasing volume energy density and thereby leads to pores that reach the surface at a specified pore volume. At a hatching distance of 400  $\mu\text{m}$  the first peak raises as expected because of the lower energy density. Furthermore, a smaller peak can be detected at about 80 to 120  $\mu\text{m}$ . This result can be explained by the development of channel like structures between the scan tracks. A single scan track has the width of the molten line by the laser beam. With the used equipment the laser beam has a spot diameter of 200  $\mu\text{m}$ . Using standard parameters these tracks overlap in order to create dense structures. The critical value when two parallel tracks lose contact and form small channels between each other seems to be a hatching distance of 300-400  $\mu\text{m}$ . This implies a width of a single scan track of around 300  $\mu\text{m}$ . The observation, that the real molten scan track is wider than the spot diameter is also made by [20]. It can be explained by a Gaussian distribution of the laser beam's energy which causes an energy input even beyond the spot diameter. Thus, a wider welding bead than the spot diameter results. A further increase of hatching distance supports the theory of forming pore channels between the scan tracks. At a hatching distance of 500  $\mu\text{m}$  the peak for bigger pores lies at around 170  $\mu\text{m}$ , which is the result of the bigger gap between the scan tracks. At 600  $\mu\text{m}$  the peak

grows further and the mean pore size reaches about 300  $\mu\text{m}$ . These results show that by increasing the hatching distance, specified levels of porosity and pore size can be obtained. Thus, a variance of hatching distance allows a porosity in the range of 7.36 % up to 36.02 % and the formation of discrete pore sizes above 100  $\mu\text{m}$ .

Increasing the layer thickness leads to a porosity up to 11.44 % at 80  $\mu\text{m}$ . The standard layer thickness for the used material represents 20  $\mu\text{m}$ . Thus 80  $\mu\text{m}$  is four times the standard value. Significant changes occur at layer thicknesses of 60  $\mu\text{m}$  and above. It seems to be possible to create a completely melted pool even with a laser thickness of 40  $\mu\text{m}$ . That means that the laser beam can penetrate the material in a bigger depth than the standard layer thickness of 20  $\mu\text{m}$ . The penetration depth is a characteristic value for each combination of laser type and powder [21]. In this case it can be concluded that the penetration depth at least is sufficient to melt two layers in order to build dense structures. When porosity starts to occur at 60  $\mu\text{m}$  it consists of both open and closed pores as expected from the former observations. The closed pores reach connection to the surface at 80  $\mu\text{m}$  and thus are detected by the mercury intrusion. The peaks have the shape of the known Gaussian distribution and are in the range of 10 to 20  $\mu\text{m}$ . In comparison with the other studied parameters, the layer thickness seems to have the lowest influence of porosity. The relation is not linear which contradicts the proposed inversely proportional influence of volume energy density on porosity. In addition, anisotropic material properties are expected, caused by the weak cohesion of layers. By variation of the layer thickness, there was no well defined influence on the porosity observable. Geometrically defined porosity is created by honeycomb and crossing walls structures. Analysis shows, that in comparison to parameter variations geometrically defined porosity with lattice structures leads to a higher overall porosity (up to 66.56 % for honeycombs and 67.14 % for crossing walls; Figure 6, Figure 7). Obviously lower wall thicknesses lead to higher porosity, which is proven by the results. The porosity increases according to the pore sizes selected in the configuration. This means that the porosity clearly results from the defined lattice structure and not from other effects such as formation of pores caused by a lower volume energy density.

Comparing the experimentally determined porosity of the honeycomb structure with the calculated (theoretical) porosity, a good approximation of these two values can be observed especially for pore sizes above 300  $\mu\text{m}$ . A closer look at the honeycomb structures shows that at a designed pore size of 200  $\mu\text{m}$  both samples with 100 and 200  $\mu\text{m}$  wall thickness show a lower value in real porosity than in theoretical (Figure 8). This can be explained by consideration of the microscopic images on Figure 10. In the pore channels not molten grains can be observed, which stick to the created walls and partially close those channels. The manufacturing of thin walls of only 100 or 200  $\mu\text{m}$  is limited through the laser focus diameter of 200  $\mu\text{m}$ . Thus, more material than desired is molten and sticks to the walls, which is also observed by [20] and occurs in the same manner during the variation of the parameter hatching distance. Lattice structure configurations with larger theoretical pore sizes show well developed pore channels. In these cases the obtained values of porosity exceed the theoretical ones. This can be explained by additional pore volume formed in the thin walls, which appears because of the missing overlapping in scan tracks, which normally supports dense structures. The pore size distribution supports this assumption. At a configuration with designed pore sizes of 200  $\mu\text{m}$  and wall thickness of 100  $\mu\text{m}$  (H1) two peaks can be identified: one at the desired pore size of 200  $\mu\text{m}$  and another one at lower values (around 15  $\mu\text{m}$ ). The peak in the lower region seems to be caused by a lower volume energy density as it is observed at geometrically undefined porosity.

Configuration H2 shows a significant peak close to its theoretical pore size value. A further increase of the honeycomb pore size (H3) does not lead to a significant pore size using mercury intrusion porosimetry. This is caused by the limitations of the measurement technique at about 300  $\mu\text{m}$ . Above this pore size the mercury can intrude in the pores without any additional pressure and thus the pores cannot be detected by this measurement method. Using microscopic analysis for larger pores it can be concluded, that even pore sizes of 300  $\mu\text{m}$  and above can be manufactured accurately with selective laser melting. The walls are formed properly, but several grains of not molten powder seem to stick on the walls of the thin structures. This results in a smaller effective diameter of the pore channels. Using 200  $\mu\text{m}$  wall thickness, those grains on the inner surface of pore channels become less. Hence, a better correlation between obtained and designed pore sizes is given at 200  $\mu\text{m}$  wall thickness. The honeycomb structure seems to be an appropriate way to fabricate porous samples with an adjustable and discrete range of pore sizes above 100  $\mu\text{m}$ . Thus, by the variation of two parameters, wall thickness and desired pore size, any level of porosity can be obtained through honeycomb structures. At smaller structures (wall thicknesses and pore sizes) the laser beam seems to be the limiting factor. The 200  $\mu\text{m}$  spot diameter of the laser and its Gaussian energy distribution causes small particles to stick on the walls and prohibits the manufacturing of smaller channels [22].

By using the crossing walls structure, similar results are obtained. The total porosity increases with higher selected values of theoretical pore size and shows lower values when using larger wall thicknesses. This relationship can be found through all tested specimens. However, the obtained porosity lies below the theoretical porosity. This can be explained by additional smaller pores in the xy-plane. The used honeycomb structure consists only of pores in the z direction but the crossing walls structure is designed to contain also pores in x and y direction. Those have a smaller diameter which cannot be created properly due to the laser focus diameter and the penetration depth of the laser. They are partly closed and hence, the calculated porosity cannot be reached entirely. [23] mention that when forming pores by geometrically defined structures the actual porosity tends to be smaller than the calculated one as well. They explain it by rests of powder, which cannot be removed from the pore channels. This certainly contributes here to a loss in porosity as well. Considering the microscopic views (Figure 10) it can be suggested that at least for selected pore values above 100  $\mu\text{m}$  (CW2,3,5,6) the pores in z direction are formed properly. This assumption is supported by the mercury intrusion porosimetry (Figure 9). The peak at 100  $\mu\text{m}$  desired pore diameter (CW1) is not detected. This is caused by the inability to remove loose powder grains out of the narrow pore channels. The structure is too thin and gets filled by not molten powder which sticks to the walls. The small detected pores are formed by spaces between the powder grains in the pore channels. At 200  $\mu\text{m}$  (CW2) pores are formed properly. A significant peak is seen at approximately 250  $\mu\text{m}$  which is also supported by the microscopic view. Microscopic analysis show that pore sizes at crossing walls structures can be manufactured more accurately with a wall thickness of 200  $\mu\text{m}$  than with 100  $\mu\text{m}$ . The next bigger pore size (CW3) cannot be detected properly by mercury intrusion. As mentioned above the pore sizes are out of the measurement range. Based on microscopic analysis it can be expected that also larger pores can be manufactured properly. Summing up, crossing walls structure are appropriate to fabricate defined porous structures. Both the total porosity and the pore size can be manufactured at accurately defined levels, when pore sizes are larger than 100  $\mu\text{m}$  and walls are thicker than 200  $\mu\text{m}$ .

## **Conclusion**

In this study two strategies to manufacture defined porosity using selective laser melting are investigated. Geometrically undefined porosity on the one hand is obtained by a variation of exposure parameters. Geometrically defined porosity on the other hand is based on lattice structures which will be exposed by the material's standard parameters.

Through the variation of exposure parameters values of porosity between 1.75 and 36.02 % and pore sizes in the range of 1 to 50  $\mu\text{m}$  are reached. The pores show no orientation and might be useful for catalysts and absorbing materials. The best results can be obtained by the variation of the parameters scan speed and hatching distance. A well-defined and distinctive pore distribution as well as a significant relationship between the porosity and the parameter is observed. Through a variation of the hatching distance not only the highest porosity is reached but also a precise adjustment of the pore sizes in a wide range is possible. The hatching distance represents the crossover to geometrically defined porosity.

The volume energy density, including all four investigated parameters, shows a strong influence on the overall porosity. Contrary to the proposed relation an inversely proportional influence of the volume energy density on porosity cannot be verified. Each parameter variation shows a distinctive but not always linear relation regarding overall porosity. Thus, the resulting characteristics of porosity depend on which factor of the volume energy density is varied. A global proportional factor cannot be determined. Further research could focus on this topic.

Using honeycomb and crossing walls structures geometrically defined porosity can be built with pore sizes above 100  $\mu\text{m}$ . Pores of 100  $\mu\text{m}$  and larger can be manufactured accurately. Best results are obtained with a wall thickness of 200  $\mu\text{m}$ . Real pore channels are formed, which are suited to be used as filters. The obtained porosity exceeds 60 % while higher values are possible by further variation of the geometric parameters.

With respect to geometrically undefined porosity problems occur when the volume energy density is too low that welding beads and single layers lose cohesion. In this case the manufacturing of specimens is not possible anymore. Powder sticking to the walls and the removal of loose powder out of the pore channels seems to be a limitation of geometrically defined porosity. Further investigations on these topics are recommended. In addition, the analysis of strength characteristics of porous structures seems to be a promising research field in order to obtain information about the use in medical environment and light weight constructions. [13] investigate the relationship between porosity and strength, coming to the conclusion of a strong dependency. This relation is supposed to vary depending of the used parameter or lattice structure.

## **Acknowledgements**

This work was supported by the Center of Smart Interfaces "Understanding and Designing Fluid Boundaries" (CSI), an Excellence Initiative of the federal government of Germany. We would like to thank the CSI and the German research Foundation (DFG) for the funding which enabled the presented results

## References

- [1] Wang, Yan et al. (2010): Development of highly porous titanium scaffolds by selective laser melting. In: *Materials Letters* 64 (6), p. 674–676.
- [2] Coleman, S. C.; Beeré, W. B. (1975): The sintering of open and closed porosity in UO<sub>2</sub>. In: *Phil. Mag* 31 (6), p. 1403–1413.
- [3] Nikolaev, V. A. (1980): Effect of porosity on the size of surface microirregularities in the finish lathe-turning and smoothing of sintered materials. In: *Powder Metall Met Ceram* 19 (9), p. 655–659.
- [4] Zhu, H. H.; Fuh, J. Y. H.; Lu, L. (2007): The influence of powder apparent density on the density in direct laser-sintered metallic parts. In: *International Journal of Machine Tools and Manufacture* 47 (2), p. 294–298.
- [5] Kruth, Jean-Pierre et al. (2005): Benchmarking of Different SLS/SLM Processes as Rapid Manufacturing Techniques. *International Conference Polymers & Moulds Innovations*. Gent, Belgium, April 20-23.
- [6] Simchi, A.; Petzoldt, F.; Pohl, H. (2003): On the development of direct metal laser sintering for rapid tooling. In: *Journal of Materials Processing Technology* 141 (3), p. 319–328.
- [7] Reinhart, G.; et al. (2010): Potentials of generative manufactured components for gaining resource efficiency of production facilities. In: R. Neugebauer (Ed.): *Sustainable production for resource efficiency and ecomobility: Manufacturing Colloquium*, Vol. 54. *International Chemnitz Manufacturing Colloquium*. Chemnitz, September 29-30, p. 703–710.
- [8] Tsinoglou, D. N. et al. (2009): A simplified model for natural-gas vehicle catalysts with honeycomb and foam substrates. In: *Proceedings of the Institution of Mechanical Engineers, Part D: Journal of Automobile Engineering* 223 (6), p. 819–834.
- [9] Heikkinen, Maire S. A.; Harley, Naomi H. (2000): Experimental Investigation of Sintered Porous Metal Filters. In: *Journal of Aerosol Science* 31 (6), p. 721–738.
- [10] Gu, Dongdong; Shen, Yifu (2008): Processing conditions and microstructural features of porous 316L stainless steel components by DMLS. In: *Applied Surface Science* 255 (5, Part 1), p. 1880–1887.
- [11] Kruth, Jean-Pierre et al. (2005): Binding Mechanisms in Selective Laser Sintering and Selective Laser Melting. In: *Rapid Prototyping Journal* 11 (1), p. 26–36.
- [12] Thijs, Lore; et al. (2010): A study of the microstructural evolution during selective laser melting of Ti-6Al-4V. In: *Acta Materialia* 58 (9), p. 3303–3312.
- [13] Mullen, Lewis; et al. (2008): Selective Laser Melting: A regular unit cell approach for the manufacture of porous, titanium, bone in-growth constructs, suitable for orthopedic applications. In: *J. Biomed. Mater. Res* 89B (2), p. 325–334.
- [14] Stamp, R.; et al. (2009): The development of a scanning strategy for the manufacture of porous biomaterials by selective laser melting. In: *Journal of Materials Science: Materials in Medicine* 20 (9), p. 1839–1848.
- [15] Standard DIN EN ISO 2738, 2000-02-00: Sintered metal materials, excluding hardmetals - Permeable sintered metal materials - Determination of density, oil content and open porosity.
- [16] Jena, Akshaya; Gupta, Krishna (2002): Characterization of Pore Structure of Filtration Media. In: *Fluid Particle Separation Journal* 14 (3), p. 227–241.

- [17] Standard DIN 66133, 1993-06-00: Determination of pore volume distribution and specific surface area of solids by mercury intrusion.
- [18] Bimberg, Dieter (1991): Materialbearbeitung mit Lasern. Grundlagen und Anwendungen: Expert Verlag.
- [19] Niu, H. J.; Chang, I. T. H. (2000): Selective laser sintering of gas atomized M2 high speed steel powder. In: Journal of Materials Science 35 (1), p. 31–38.
- [20] Lohfeld, S.; et al. (2010): A method to fabricate small features on scaffolds for tissue engineering via selective laser sintering. In: JBiSE 03 (02), p. 138–147.
- [21] Fischer, P. et al (2003): Sintering of commercially pure titanium powder with a Nd:YAG laser source. In: Acta Materialia 51 (6), p. 1651–1662.
- [22] Li, Ruidi et al. (2010): 316L Stainless Steel with Gradient Porosity Fabricated by Selective Laser Melting. In: Journal of Materials Engineering and Performance 19 (5), p. 666–671.
- [23] Williams, Jessica M. et al. (2005): Bone tissue engineering using polycaprolactone scaffolds fabricated via selective laser sintering. In: Biomaterials 26 (23), p. 4817–4827.